Vol 18 No 7, July 2009
1674-1056/2009/18(07)/2953-08

Chinese Physics B

© 2009 Chin. Phys. Soc.
and IOP Publishing Ltd

First-principles study on the magnetism of different dimensional Ru systems*

Zhu Qiu-Xiang(朱秋香), Pang Hua(庞 华)†, and Li Fa-Shen(李发伸)

Key Laboratory for Magnetism and Magnetic Materials of the Ministry of Education, Lanzhou University, Lanzhou 730000, China

(Received 21 October 2008; revised manuscript received 24 November 2008)

The magnetism, the magnetocrystalline anisotropy and the optical properties of the monolayer and atomic chain of 4d transition-metal Ru are investigated by using the full-potential linearized-augmented-plane-wave method in a generalized gradient approximation. The magnetic moments are 1.039 μ_B/atom and 1.130 μ_B/atom for the monolayer and atomic chain, respectively. Both systems have large magnetocrystalline anisotropy energy (MAE). The magnetic easy axis is normal to the monolayer and perpendicular to the chain axis in the atomic chain. The optical properties of the two low-dimensional Ru systems are investigated by calculating the complex optical conductivity tensor. Both systems exhibit anisotropy in photoconductivity, especially for the atomic chain. The physical origins of MAE and photoconductivity are studied based on electronic structures. It is found that the changes in crystal field caused by different symmetry-breaking mechanisms in the two low-dimensional Ru systems result in MAE through spin–orbit coupling, while the anisotropy in photoconductivity mainly comes from the crystallographic anisotropy.

Keywords: first-principle, anisotropy, optical properties
PACC: 7115M, 7530G, 7820L

1. Introduction

Rapid development in magnetism at the nanometer scale during the last two decades has led to the discovery of a number of fundamental physical phenomena, such as dimensionality-induced magnetization of non-magnetic metals, oscillatory magnetic coupling between metallic multilayers, thus arousing research interest in low-dimensional materials[1] Now the growth of nano-structured systems with desired dimensionality can be achieved at the atomic scale, which allows the study of the influence of dimensionality on material properties in great detail.[2,3] Corresponding calculations have been carried out at the same time[4−7] Among them, multilayers, monolayers and atomic chains of 3d, 4d and 5d transition metals have been attracting extensive research interest, and their mechanical properties and magnetic properties have been well discussed based on their electronic structures.[8−11] Magnetic anisotropy (MA) is one of the fundamental intrinsic properties for magnetic materials, and the origin of MA has long been an attractive subject for both experimentalists and theoreticians.[6,9,12] Photoconductivity is another property which is closely related to the electronic structures of materials. However, there are few reports about the optical properties of the atomic chain in comparison with the well studied optical or magneto-optical properties in 2D and 3D systems.[13−18] Besides, the relationship between the MA and the Kerr effect is still controversial. There are experimental reports showing that large MA can be helpful for inducing a larger Kerr angle, but there are also results indicating that the two effects seem not to be related to each other directly.[13]

In this paper, we perform first principles calculations on the magnetism, magnetocrystalline anisotropy energy (MAE) and the optical properties of the monolayer and atomic chain of 4d transition-metal Ru. We focus on the physical origins of MAE and the anisotropy of optical properties in low-dimensional Ru systems. Moreover, the relationship between the MAE and the anisotropy in optical properties in low-dimensional systems is also investigated.

*Project supported by the National Natural Science Foundation of China (Grant Nos 90505007 and 10774061).
†Corresponding author. E-mail: hpang@lzu.edu.cn

2. Computational method

All calculations are performed by using the WIEN2K package[19] in which the full-potential linear-augmented-plane-wave (FLAPW) method is implemented within the framework of the density-functional theory (DFT). The Perdew and Wang generalized gradient approximation (GGA) is employed for the exchange-correlation potential.[20] Scalar-relativistic effects are included for the band states, and the core-level states are treated fully relativistically in an atomic-like approximation. The muffin-tin (MT) radii $R_{\rm MT}$ is chosen as 2.09 a.u. for Ru. The potential and the charge density in the MT-spheres are expanded in spherical harmonics with $l_{\rm max} = 10$. The cutoff parameter $R_{\rm MT}K_{\rm max}$ for limiting the number of the plane waves is equal to 7.0. The magnitude of the largest vector $G_{\rm max}$ in charge density Fourier expansion is 14.0.

The free-standing atomic chain is simulated by a two-dimensional array of infinite long straight atomic wires. The nearest wire–wire distance is carefully chosen to decouple the neighbouring wires. Systematic calculations prove that a separation of 13 Å is large enough, since the electronic structure, the magnetic properties and the MAE from our test calculations with a larger separation of 15 Å are nearly identical to that obtained with the wire–wire distance of 13 Å. The isolated atomic layer is also modeled according to the standard supercell approach. The layers are formed as the hexagonal close-packed structure but the layer-layer separation between the neighbouring layers is set to be 12 Å to avoid the interlayer interactions. The atomic positions in each low-dimensional model are fully relaxed by using the conjugate gradient method until the force on each atom after relaxation is smaller than 1.0 mRy/a.u. Table 1 displays the optimized lattice parameters in this paper. For the atomic chain, where a comparison is possible to be made, our values are quite close to the reported ones.[9] The lattice constants for the 3D bulk come from the experimental results.[21]

Table 1. Optimized lattice constant, calculated magnetic moments and MAE.

systems	lattice constant/Å		spin moment/$\mu_{\rm B}$	MAE/(meV/atom)
atomic chain	$a = b = 13.000$	$c = 2.243$	1.130	9.547
monolayer	$a = b = 2.534$	$c = 12.000$	1.039	–3.468
bulk	$a = b = 2.710$	$c = 4.280$	0.000	–0.027

Since the MAE is crucially dependent on the details of the Brillouin zone (BZ) integration, a closer look at the convergence of the MAE with respect to the number of k-points is needed. We have performed a series of test calculations and find that the MAE converges reasonably with a 13×13×65 k grid (693k-points in the irreducible Brillouin zone) for an Ru atomic chain. And the 30×30×5 k grid and 45×45×25 k grid are large enough for the convergence of MAE in monolayer and bulk models, respectively.

Table 2. Variations of ω_{xx} and ω_{zz} with the number of k-points in the atomic chain.

k-points	10000	20000	30000	45000	60000
$\omega_{xx}/{\rm s}^{-1}$	0.0038	0.0033	0.0032	0.0034	0.0033
$\omega_{zz}/{\rm s}^{-1}$	5.1335	4.3367	4.1154	4.3029	4.1880

The convergence of the optical properties with respect to the number of k-points is also checked carefully. Listed in Table 2 are the variations of plasma frequencies ω_{xx} and ω_{zz} with the number of k-points in the Ru atomic chain when magnetized along the z-axis. It is found that 60000 k-points are large enough for the convergence of the calculated optical spectra for the Ru atomic chain. Using the same testing method, we find that 60000 k-points are also enough for the convergence in the Ru monolayer.

3. Results and discussion

3.1. Magnetic moment

The magnetic moments of the three Ru systems are also given in Table 1. The bulk Ru is nonmagnetic. But the appearance of magnetism in reduced dimensions is obvious. The magnetic moments are 1.039 $\mu_{\rm B}$ and 1.130 $\mu_{\rm B}$ per atom in the Ru monolayer and the Ru atomic chain, respectively. The magnetism

in reduced dimensions is caused by the symmetry breaking in the neighbourhood of the Ru atom, which brings about a reduction in the kinetic energy of electrons and consequently results in a band narrowing.[9] Since the electrons become more localized, they have more opportunities for exchange, thereby resulting in exchange-splitting. Figure 1 shows the calculated total electronic densities of states (DOSs) for all the models mentioned above. We can see that the exchange splittings between the majority states and minority states are obvious for the Ru atomic chain and monolayer, which induces the spin polarization, hence spontaneous magnetization in the low-dimensional systems. According to the calculated spin-resolved occupation numbers of each orbital, we find that the magnetic moments mainly come from the 4d electrons. And the 4d orbitals with spatial distribution along the chain axis account for the magnetic moment in the atomic chain, while those distributed

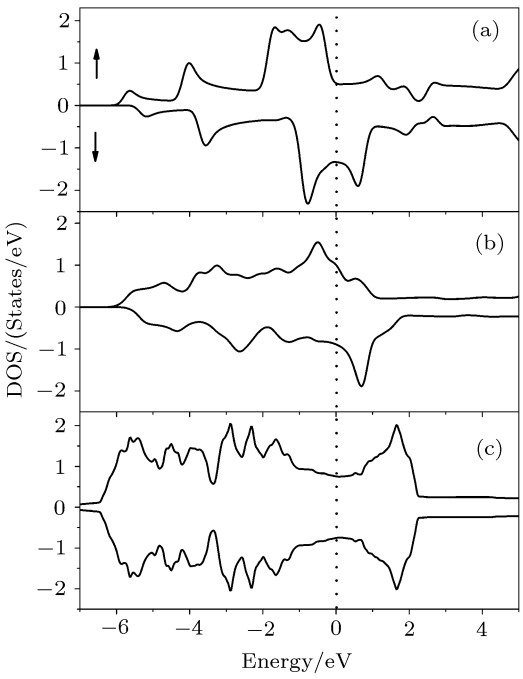


Fig.1. Total densities of states (DOSs) of three different dimensional Ru systems, i.e. atomic chain (a), monolayer (b), and bulk (c), near the Fermi level, whose position is marked with a vertical dash line.

in the direction perpendicular to the atomic layer contribute most to the monolayer. We also calculate the magnetic moments of two-layered and multi-layered Ru model systems and find no magnetism in them. These calculations further prove the importance of symmetry breaking due to the reduced dimensions to the polarization of 4d electrons.

3.2. MAE

The MAE of a magnetic solid is a difference in total electronic energy between two magnetization directions, or the energy required to rotate the magnetization from one direction to another. MAE, as a ground-state property, can be obtained from two independent self-consistent relativistic total-energy calculations in two different magnetization directions, n_1 and n_2. The difference between the corresponding ground-state energies is expressed as the MAE of the two directions: $\mathrm{MAE} = E^{n_1} - E^{n_2}$. In the present paper, the magnetization directions are defined as the z-axis ([0001] crystal direction) and the x-axis ([1100] crystal direction). So the z-axis is parallel to the axis of the atomic chain and perpendicular to the monolayer plane. The calculated MAEs for three Ru systems are listed in Table 1, where the positive value means that the easy direction is along the x-axis and the negative value means that the z-axis is the easy axis. The MAE is 9.547 meV/atom in the Ru atomic chain, indicating that the easy magnetic axis is perpendicular to the chain axis. Our calculation is consistent with the reported result in Ref.[9]. The

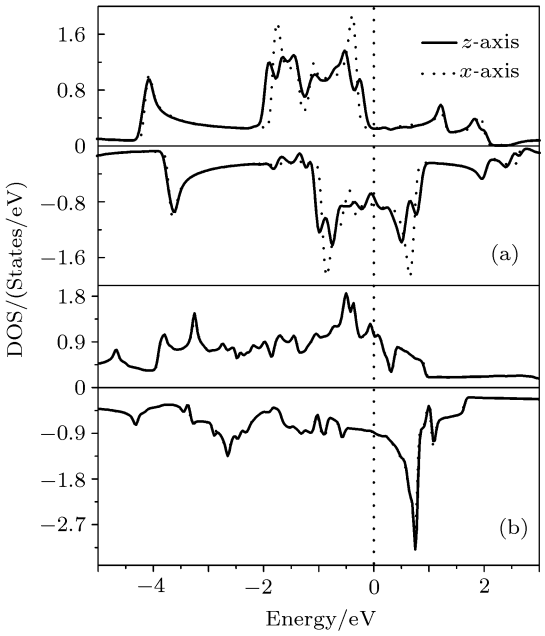


Fig.2. Total DOSs of the 1D atomic chain (a) and 2D monolayer (b) when magnetized along the z-axis (solid lines) and x-axis (dotted lines), where the Fermi level is indicated with a vertical dashed line.

MAE in the monolayer is –3.468 meV/atom, which means that the easy magnetization axis is perpendicular to the plane. This result also accords with the reported easy direction in the metallic monolayer.[11,22] Since the MAE is quite sensitive to the details of

the electronic structure, we show the calculated total DOSs with spin–orbital (SO) coupling along the z axis (solid lines) and the x axis (dot lines) for the two low-dimensional models in Fig.2. Clearly, under different magnetization directions, the variations in the total DOS of the atomic chain (Fig.2(a)) are much more prominent than those of the monolayer (Fig.2(b)), which may be associated with the larger MAE in the atomic chain.

It is well known that relativistic electron spin–orbital (SO) coupling is the fundamental origin of the orbital magnetization, as is the MAE in solids. We then calculate the partial DOS including SO coupling along the x-axis (right column) and z-axis (left column), and show the results of 4s, 4p and 4d states in Fig.3. Due to the strong SO coupling of 4d shell compared with those of 4s and 4p shells, the differences in DOS profiles of 4d states under the two magnetization directions are quite distinct. All three partial 4d orbitals are more localized when magnetized along the x-axis than along the z-axis, especially for the d_{z^2} and d_{xz+yz} orbitals. This is reasonable if the limitation of electron mobility along the x and the y directions in 1D system is taken into consideration. The localized states may be more sensitive to the asymmetry of the crystal field of the neighbour atoms and contribute more to the MAE.

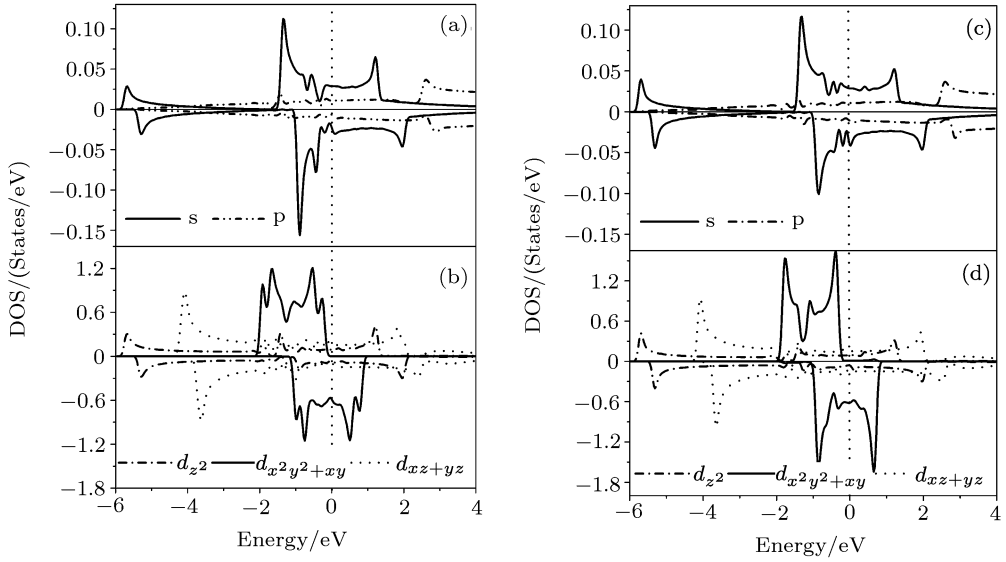


Fig.3. Partial DOSs of the atomic chain when magnetized along the z-axis ((a) and (b)), and along the x-axis ((c) and (d)).

It is hard to point out the contribution of each 4d orbital to MAE directly and quantitatively from the DOS plots. We further calculate the contributions of individual 4d orbitals to the MAE as a function of band filling q (number of valence electrons), and the results are shown in Fig.4. The Fermi energy corresponds to $q = 8$ for the Ru atomic chain. Then the curves in Fig.4 are obtained by varying the number of valence electrons Δq (i.e. the position of the Fermi level) in the manner of a rigid-band model. It is found that at the Fermi level, the d_{z^2} orbital drives the magnetic moment to the direction of the chain axis, while the $d_{x^2y^2+xy}$ and d_{xz+yz} orbitals tend to drive the moment to the direction of the chain radius. Thus the competition among the three 4d orbitals determines

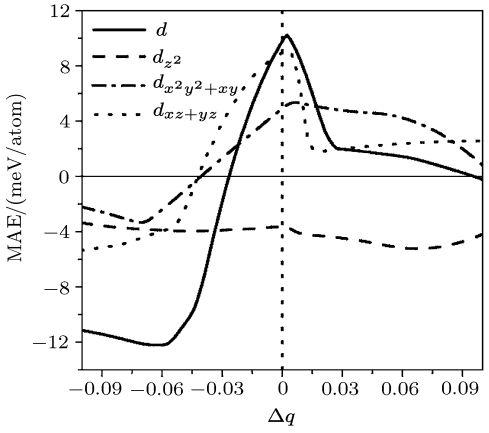


Fig.4. Curves for MAE for 4d orbitals as a function of band filling Δq in the atomic chain, where the Fermi energy corresponds to $\Delta q = 0$, marked with a vertical line.

the MAE at the Fermi level. Clearly, the MAE profile of the d_{xz+yz} orbital is similar to that of the total 4d orbital around $\Delta q = 0$, indicating that the d_{xz+yz} orbital contributes most to the MAE in the atomic chain. It is also worth noting that the MAE experiences a large fluctuation around the Fermi level, which enlightens us on modulating the MAE in the atomic chain by controlling the number of valence electrons.

The situation in the monolayer is a little bit complicated. Magnetization along the x-axis lowers the symmetry of the system. The degeneracy of the 4d shell is removed, and the five 4d orbitals are d_{xy}, $d_{x^2y^2}$, d_{xz}, d_{yz} and d_{z^2} as shown in Fig.5, where the left panels show the partial states including SO coupling along the z-axis, and the right panels correspond to those that are magnetized along the x-axis. Clearly, the SO splittings are quite different in the two magnetization directions, hence inducing large MAE in the monolayer. According to electronic structure and band-filling arguments, we find that the d_{z^2} orbital is most crucial to the MAE in the 2D monolayer.

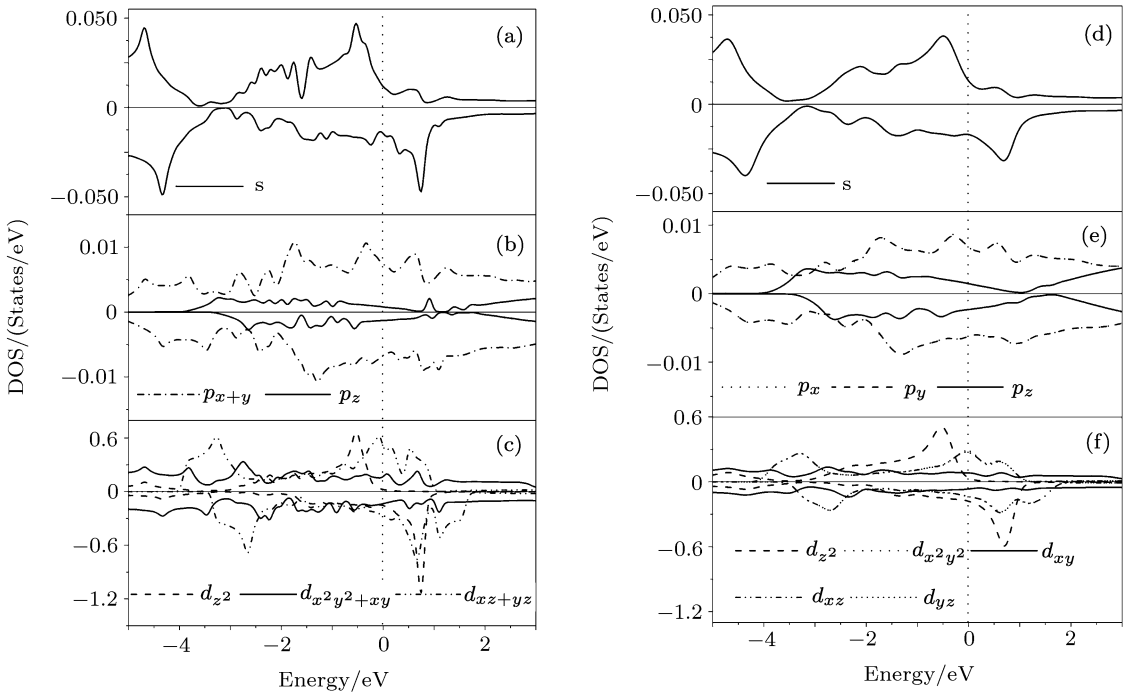


Fig.5. Curves for partial DOS of the Ru monolayer when magnetized along the z-axis ((a), (b) and (c)) and along the x-axis ((d), (e) and (f)).

3.3. Optical properties

Now we come to investigate the optical properties of the two low-dimensional Ru systems. The complex optical conductivity tensor $\sigma_{\alpha\beta}(\omega) = \sigma_1^{\alpha\beta}(\omega) + \mathrm{i}\sigma_2^{\alpha\beta}(\omega)(\alpha, \beta = x, y, z)$ is the basic spectral quantity of metals. The tensor components can be separated into electronic transitions appearing from band to band (interband electronic transitions) and electronic transitions occurring within the same band (intraband electronic transitions). For the diagonal tensor components, both terms are important and should be considered simultaneously. As to the off-diagonal tensor components, the intraband contribution is very small and usually neglected in the case of magnetically ordered materials.

The optical conductivity tensor $\sigma_{\alpha\beta}$ is related to the dielectric tensor $\varepsilon_{\alpha\beta}$ through $\varepsilon_{\alpha\beta}(\omega) = \delta_{\alpha\beta} + 4\pi\mathrm{i}\sigma_{\alpha\beta}(\omega)/\omega$. For the interband transitions, the imaginary part of the dielectric function is calculated directly from the electronic structure through the joint DOS and the matrix elements of the momentum $\boldsymbol{p}$ between occupied and unoccupied eigenstates

$$\varepsilon_2^{\alpha\beta}(\omega) = 4\pi^2 e^2 \sum_{Knn'} \langle Kn\,|p^\alpha|\,Kn'\rangle \langle Kn'\,|p^\beta|\,Kn\rangle (f_{Kn} - f_{Kn'})\delta(E'_{Kn} - E_{Kn} - \hbar\omega)/\Omega m^2\omega^2, \qquad (1)$$

where e is the electron charge, m is the mass, Ω is the volume of the crystal, f_{Kn} is the Fermi distribution function and $|Kn\rangle$ is the crystal wave function corresponding to the nth eigenvalue E_{Kn} with the crystal wave vector K.[23] The real part of the dielectric function is calculated via the Kramers–Kronig transformation. The imaginary and the real parts of the dielectric function for the intraband transitions are $\varepsilon_2^{\alpha\beta}(\omega) = \Gamma\omega_{p,\alpha\beta}^2/[\omega(\omega^2+\Gamma^2)]$ and $\varepsilon_1^{\alpha\beta}(\omega) = 1-\omega_{p,\alpha\beta}^2/(\omega^2+\Gamma^2)$, respectively where Γ is the lifetime broadening and $\omega_{p,\alpha\beta}$ is the plasma frequency, which is given by

$$\omega_{p;\alpha\beta}^2(\omega) = \hbar^2 e^2 \sum_{Kn} \langle Kn\,|p^\alpha|\,Kn'\rangle \left\langle Kn'\left|p^\beta\right|\,Kn\right\rangle \delta(E_{Kn}-E_{\rm F})/\pi m^2, \tag{2}$$

with $E_{\rm F}$ being the Fermi energy.

Figure 6 displays the calculated real and imaginary parts of the optical conductivity tensor components σ_{xx} and σ_{zz} of the two low-dimensional Ru systems when magnetized along the x-axis and the z-axis. The calculated off-diagonal components of the optical conductivity tensor of the two systems are about 20 orders of magnitude smaller than the diagonal components, so we neglect them in the following. We find that the spectra of photoconductivity in the two systems are quite different from each other. Taking into account both intraband and interband transitions, the spectra of the two systems show typical metallic characters, and there are at least three features that are noticeable: First, the components of the optical conductivity tensors along the crystal symmetry breaking direction, such as the σ_{xx} component in the atomic chain and σ_{zz} component in the monolayer, are in the ultraviolet range for both systems. Second, the photoconductivity peaks are broader and higher for the monolayer in the low energy range than those for the atomic chain. Third, the spectra of photoconductivity show a shoulder at about 1eV in the monolayer, but it is absent in the atomic chain in the same energy range.

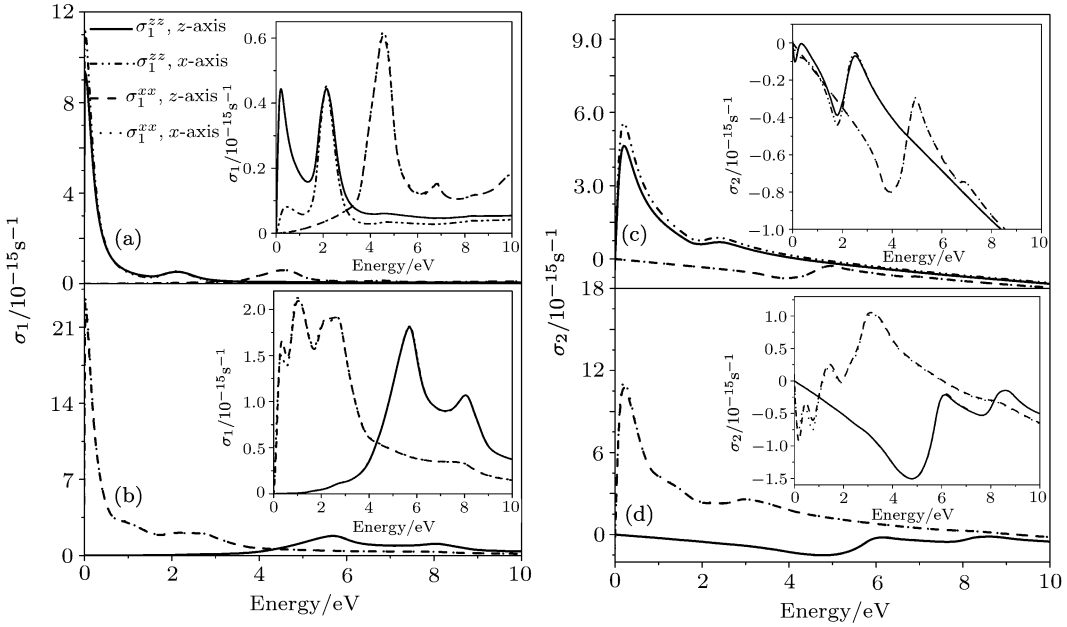


Fig.6. Curves for the real part and imaginary part of diagonal optical conductivities when magnetized along different directions, where panels (a) and (c) show real parts and imaginary parts of σ^{zz} and σ^{xx} components for Ru atomic chain respectively, panels (b) and (d) indicate the ones for Ru monolayer, and the insets are for the corresponding interband contributions.

The first feature can be well understood from the electronic structures of the two systems. In 1D and 2D systems, the electron densities distributed along the symmetry breaking direction, such as the $d_{x^2y^2+xy}$ band in the atomic chain and d_{z^2} band in the monolayer, show localized features. This kind of localization reduces the electron speed at the Fermi level, which essentially affects carrier mobility.[24] As a result, the plasma frequency, which is proportional to the Fermi speed, decreases simultaneously. For example, as depicted in Table 2, ω_{xx} is 0.0033 in the atomic chain, three orders of magnitude smaller than $\omega_{zz}(\omega_{zz} = 4.1880)$, indicating a much reduced

intraband transition probability for the related bands. So the σ_{xx} component in the atomic chain and the σ_{zz} component in the monolayer mainly come from the interband transitions, which induce photoconductivity peaks in the ultraviolet range. The second feature can be explained analogously. The monolayer has a larger number of states when including SO coupling than the atomic chain near the Fermi level, as shown in Fig.2. This will induce higher transition probabilities hence larger photoconductivity in the monolayer. What is more, the sharp photoconductivity peaks of the atomic chain compared with those in the monolayer could be attributed to the more localized electronic structure of the atomic chain. To understand the appearance of the shoulder in the photoconductivity spectra of the monolayer, we switch to the investigation of the contributions of the interband transitions to the photoconductivity. When involving only the interband transitions, the difference in the photoconductivity spectrum between the two low dimensional systems is quite distinct as shown in the insets of Fig.6. In a low-energy range, instead of two peaks in the spectra of the atomic chain, there are three peaks in the spectra of the monolayer. Clearly, the peak around 1.0 eV, which is special for the monolayer, causes the shoulder in the spectra.

We then focus on the anisotropy of the optical properties of the two low-dimensional Ru models. As stated in Ref.[25], there are two contributions to the anisotropy of optical properties. First, a purely magnetocrystalline anisotropy contribution stemming from the variation of off-diagonal optical conductivity with the orientation of the orbital moment. Second, a purely crystallographic anisotropy contribution originating from the difference in diagonal optical conductivity. Considering the very small variations in the off-diagonal components of the optical conductivity tensors under different magnetization directions, the anisotropy of photoconductivity is attributed mainly to the crystallographic anisotropy for both low-dimensional systems.

The explanation for the above behaviour may be made clearer in terms of electronic structure. In a low-dimensional system, owing to the asymmetric crystal field, the spatial distributions of valence orbitals are anisotropic. Including SO coupling to these orbitals results in orbital magnetic anisotropy hence MAE. In addition, the electronic transitions among these states result in the anisotropy in the optical conductivity tensor. Since the crystallographic anisotropy in the atomic chain is quite different from that in the monolayer, the atomic chain behaves more anisotropically in the optical properties. As shown in Fig.6, obvious anisotropy in the optical conductivity only appears in the Ru atomic chain though the atomic chain and the monolayer, and each have a large MAE. Hence the anisotropies of optical properties and the MAE do not necessarily have the same origins, especially in low-dimensional systems, where the crystallographic anisotropy is more important in inducing the anisotropy of photoconductivity. For example, we see from Fig.6 that the σ^{zz} components show distinct anisotropies at about 0.3 eV in the spectra of the atomic chain. A closer investigation on the electronic structure indicates that the peak at 0.3 eV is most probably caused by the electronic transitions between different 4d bands, among which the $d_{x^2y^2+xy}$ band, whose DOS profiles under the two magnetization directions are quite different, makes the most contributions. As mentioned above, the easy axis is determined by the competition among the three 4d orbitals near the Fermi energy, though we see that a certain individual orbital controls the anisotropy of optical conductivity in the atomic chain. As to the monolayer, electronic transitions between 4p and 4d states and those between different 4d bands near the Fermi level create all of the three photoconductivity peaks below 4.0 eV. Though the differences between the 4p and 4d DOS profiles are quite obvious under different magnetization directions which do cause large MAE, the anisotropy in photoconductivity is almost negligible in the Ru monolayer. This observation is helpful for understanding some experimental results where large Kerr rotation is not always accompanied with large MAE in some materials.[13]

4. Conclusions

We report on a first principles study on the magnetic and the optical properties of low-dimensional Ru systems by using the FLAPW method. We find that nonmagnetic bulk Ru turns out to be magnetic when reducing the dimensions. The magnetism increases with the reduction in dimension and the magnetic moments are 1.130 and 1.039 μ_B/atom in the Ru atomic chain and the Ru monolayer, respectively. The differences in the local neighbourhood environment between Ru atoms and crystal-filled splitting under dif-

ferent magnetization directions result in anisotropies in magnetism and photoconductivity through SO coupling. The easy axis is perpendicular to the atomic chain axis and the monolayer, but the MAE is much larger in the former case. Based on the electronic structures and the evolutions of MAE with the band filling, we find that the competition among individual 4d orbitals determines the easy axis in both systems. The atomic chain also shows distinct anisotropy in photoconductivity, which is ascribed mainly to the crystallographic anisotropy due to symmetry breaking in low-dimensional systems.

Acknowledgment

Computer resources were provided by Key Laboratory for Magnetism and Magnetic Materials of the Ministry of Education Lanzhou University, China.

References

[1] Himpsel F J, Ortega J E, Mankey G J and Willis R F 1998 *Adv. Phys.* **47** 511
[2] ZhangY and Dai H J 2000 *Appl. Phys. Lett.* **77** 3015
[3] Gambardella P, Blanc M, Brune H, Kuhnke K and Kern K 2000 *Phys. Rev.* B **61** 2254
[4] Zhu Z L, Gu J H and Jia Y 2007 *Physica* B **387** 190
[5] Ayuela A, Raebiger H, Puska M J and Nieminen R M 2002 *Phys. Rev.* B **66** 035417
[6] Hong J S and Wu R Q 2003 *Phys. Rev.* B **67** 020406(R)
[7] Delin A and Tosatti E 2004 *Surface Science* **566–568** 262
[8] Tung J C and Guo G Y 2007 *Phys. Rev.* B **76** 094413
[9] Mokrousov Y, Bihlmayer G, Heinze S and Blügel S 2006 *Phys. Rev. Lett.* **96** 147201
[10] Delin A and Tosatti E 2003 *Phys. Rev.* B **68** 144434
[11] Garreau G, Beaurepaire E, Ounadjela K and Farle M 1995 *J. Magn. Magn. Mater.* **148** 143
[12] Uba L, Uba S, Antonov V N, Yaresko A N, Ślęzak T and Korecki J 2000 *Phys. Rev.* B **62** 13731
[13] Kautzky M C and Clemens B M 1995 *Appl. Phys. Lett.* **66** 1279
[14] Uba L, Uba S, Yaresko A N, Perlov A Ya, Antonov V N and Gontarz R 1999 *J. Magn. Magn. Mater.* **193** 159
[15] He W, Zhan Q F, Wang D Y, Chen L J and Cheng Z H 2008 *Chin. Phys.* B **17** 1902
[16] Marutzky M, Barkow U, Weber S, Schoenes J and TrocR 2006 *Phys. Rev.* B **74** 205115
[17] Ouyang C Y, Xiong Z H, Ouyang Q Z, Liu G D, Ye Z Q and Lei M S 2006 *Chin. Phys.* **15** 1585
[18] Uba L, Uba S, Antonov V N Yaresko A N and Gontarz R 2001 *Phys. Rev.* B **64** 125105
[19] Blaha P, Schwarz K, Sorantin P and Trickey S B 1990 *Comput. Phys. Commun.* **59** 399
[20] Perdew J P, Burke K, Ernzerhof M 1996 *Phys. Rev. Lett.* **77** 3865
[21] Mehl M J and Papaconstantopoulos D A 1996 *Phys. Rev.* B **54** 4519
[22] Abe H, Amemiya K, Matsumura D, Kitagawa S, Watanabe H, Yokoyama T and Ohta T 2005 *J. Magn. Magn. Mater.* **302** 86
[23] Han S H, Persson C, Hasoon F S, Al-Thani H A, Hermann A M and Levi D H 2006 *Phys. Rev.* B **74** 085212
[24] Kulatov E, Nakayama H, Mariette H, Ohta H and Uspenskii Y A 2002 *Phys. Rev.* B **66** 045203
[25] Oppeneer P M, Galanakis I, James P, Eriksson O and Ravindran P 1999 *J. Magn. Sot. Jpn.* **23** 21